Deep Characterization of Multimodal Brain Changes Across Pregnancy and the Postpartum: A Case Study

By

Sanjana Ravi

Thesis

Submitted to the Faculty of the

Graduate School of Vanderbilt University

In partial fulfillment of the requirements

For the degree of

MASTER OF SCIENCE

in

Psychology

May 12, 2023

Nashville, Tennessee

Approved:

Kathryn L. Humphreys, Ph.D.

Antonia N. Kaczkurkin, Ph.D.

TABLE OF CONTENTS

Page

LIST OF TABLES

LIST OF FIGURES

CHAPTER I

Introduction

The peripartum period is characterized by changes across multiple domains, including physiology, cognition, and socio-emotional functioning. Physically. the size of the uterus increases by about 5 times its preconception size (Shagana et al., 2018). However, changes are not limited to uterine growth. For instance, in pregnancy blood volume begins to rise at 6-8 weeks and, relative to non-pregnant comparisons, by 40 weeks increases by as much as 50% (Boeldt & Bird, 2017). Many pregnant individuals report a range of cognitive functioning changes, commonly referred to as "pregnancy brain" or "baby brain," which includes a constellation of features including increased forgetfulness (Casey et al., 1999), difficulty concentrating (Brett & Baxendale, 2001), inability to maintain attention (Brett & Baxendale, 2001), and poor effortful processing (Henry & Rendell, 2007). In terms of socio-emotional functioning, pregnant individuals tend to experience mood changes exhibiting a U-shaped pattern with negative mood (e.g., irritability and distress) increasing early in pregnancy, decreasing midway through pregnancy, and increasing again later in pregnancy, with positive mood exhibiting the inverse course (Markon et al., 2021). Importantly, non-human animal research suggests that changes in the maternal brain are occurring during the peripartum period, and may be responsible for observed behavioral differences (see Cárdenas et al., 2020, for review).

Past non-human animal work indicates that several regions of the brain undergo changes during the peripartum period. Plasticity has been documented in regions such as the lateral ventricle, pituitary, hypothalamus, nucleus supraopticus, nucleus paraventricularis, hippocampus,

subventricular zone, olfactory bulb, and medial prefrontal cortex (Hillerer et al., 2014a). Lactating rodents exhibited reduced total brain weight and hippocampal volume compared to nulliparous rodents (Hillerer et al., 2014). The alterations in functional brain networks also correspond to maternal behaviors. For example, before giving birth, the rat has an aversive response to pup odor, but at birth, this response no longer persists through activation of the medial preoptic area and ventral bed nucleus of stria terminals (Brunton & Russell, 2008). Yet, we know very little about whether these same changes are found in humans.

The first human study that investigated brain changes followed a small sample of women with (n=5) and without preeclampsia (n=9) (Oatridge et al., 2002). Though women underwent MRI scans at different stages, the primary findings indicated that total brain volume declined over pregnancy (single participants demonstrated 4.1% and 6.6% reductions from preconception to term). More recent work in 25 primiparous (i.e., pregnant for the first time) participants examined whether these changes are global or specific and found greater gray matter volume reductions in the anterior and posterior cortical midline and sections of the bilateral prefrontal and temporal cortex (Hoekzema et al., 2017). During the postpartum period, gray matter increases are posited to reverse the reductions in gray matter volume occurring in pregnancy (Kim et al., 2010). In a study on 19 biological mothers of full-term, healthy infants, gray matter volume increased from Time 1 (2-4 weeks postpartum) to Time 2 (3-4 months postpartum), particularly in the superior, middle and inferior prefrontal cortex, precentral and postcentral gyrus, superior and inferior parietal lobe, insula and thalamus (Kim et al., 2010). There is evidence that the reductions in volume are still present years after giving birth (Hoekzema et al., 2017; Martínez-García et al., 2021). In terms of functional brain changes, prior research used electroencephalogram (EEG) and functional near-infrared spectroscopy (fNIRS) to investigate

whether patterns of activity differed either due to pregnancy or across pregnancy. For instance, pregnant women in their third trimester exhibited greater neural reactivity to emotional stimuli compared to non-pregnant women (Raz, 2014). Women also exhibited greater prefrontal cortex activation and attention bias towards threatening images in their second trimester compared to their first or third trimester (Roos et al., 2011). While EEG and fNIRS offer insight into brain activity, they lack the spatial resolution provided via MRI. Using MRI enables the examination of brain network organization both functionally and structurally, including changes in constituent measures in volume (e.g., cortical thickness and surface area), and changes in white matter tracts. Importantly, concerns about the potential for MRIs to be unsafe for pregnant women and fetuses have resulted in the relative lack of research on the maternal brain in human pregnancy (Cárdenas et al., 2020), such that there is only one study that has longitudinally followed mothers from pregnancy to the early postpartum period (Oatridge et al., 2002) and another assessing women before and after, but not during, pregnancy (Hoekzema et al., 2017).

This proof-of-concept study aimed to characterize brain changes in a single subject across their pregnancy and postpartum period. We examined morphometric changes using several volume metrics (i.e., total brain volume, total gray matter volume, total white matter volume, total cortical volume, subcortical gray matter volume, and total ventricular volume) as well as constituent measures in volume (i.e., mean cortical thickness and total surface area). Further, we examined subject-specific network organization by using a personalized network assignment scheme as there is evidence to suggest that individual brain organization is qualitatively different from group-average estimates (i.e., substantial heterogeneity in cognitive maps between individuals). Using the custom atlas, we examined structural (fractional anisotropy [FA] and mean diffusivity [MD]) and functional (network coherence and network modularity) connectivity

across seven networks (i.e., attention and visual, auditory, cingulo-opercular and dorsal attention, default mode and fronto-parietal, right lateral visual, somatomotor hand, and somatomotor mouth). In line with past literature, we expected reductions across pregnancy in volume estimates, mean cortical thickness, and surface area, followed by an increase in these same metrics across the postpartum period. Given that there is no previous research work examining functional and structural connectivity changes using MRI, we refrained from making *a priori* directional hypotheses for changes in metrics obtained via these modalities and view this study as primary descriptive.

CHAPTER II

Method

2.1 Participant Characteristics

The participant was a right-handed, White, female, aged 32 years old and pregnant for the first time at the onset of the study. Subject was recruited from the Vanderbilt University community. Participant had no known medical history of neurological injury or impairment. Study procedures were approved by the Vanderbilt University Institutional Review Board and in consultation with the director of the human imaging core at the Vanderbilt University Institute of Imaging Science (VUIIS), a pediatrician and bioethicist, and a maternal-fetal medicine obstetrician. Participant provided informed consent prior to participation. There are no known risks to the mother or fetus associated with repeated fMRI scans given it contains no non-ionizing radiation (Levine, 2013).

2.2 MRI Data Acquisition

The participant completed a total of 9 fMRI scans (5 during pregnancy and 4 in the postpartum period) at VUIIS using a Philips Ingenia Elition 3.0 T X equipped with a 32-channel head coil. The pregnancy scans took place at 8, 10, 31, 35, and 37 weeks gestation and the postpartum scans took place at 6, 8, 12, and 15 months postpartum (noted in figures as 68, 76, 96, and 106 weeks gestation). The participant declined to scan during second trimester while waiting on additional expert guidance on safety of the procedure. Further, the first postpartum scan was delayed until 6 months postpartum due to research-related closures in response to the COVID-19 pandemic.

Participant completed an MRI safety screening form prior to each scan and was instructed to refrain from any caffeine intake the day of the scan (see Wu et al., 2014). Hearing protection was provided to the participant. Additionally, all noise levels in scans during pregnancy are below FDA thresholds for MRI-related noise exposure during pregnancy (Tocchio et al., 2015). As an added precaution, participant was fitted with a noise-attenuating foam pad around her abdomen during the pregnancy scans to reduce fetal noise exposure.

T1-weighted (1.1x1.1x1.2mm^3 voxel, flip angle = 9 degrees, FOV = 270x253x204mm, TR = 6.7ms, TE = 3.1ms) and T2-weighted (0.6x0.8x2.5mm^3 voxel, flip angle = 90 degrees, FOV = 240x191x1125mm, TR = 6000ms, TE = 80ms) anatomical images, resting-state fMRI (3x3mm^2 voxel, slice thickness = 3.5mm, FOV = 240x240mm, multiband factor = 0, SENSE = 2, TR = 2000ms, TE = 35ms), and diffusion weighted images (DWI; TR = 4050ms, TE = 92ms, FOV = 240x240, resolution = 2x2mm^2, slice thickness = 2mm, multiband factor = 3, number of prescribed slices = 63). For DWI, a total of 12 non-diffusion weighted (b0) volumes were acquired, along with 23 diffusion-weighted volumes/directions at b-value = 500, 47 at b-value = 1500, and 70 at b-value = 2500. All modalities were obtained at each scan with the exception of the second pregnancy scan (i.e., 10 weeks gestation) whereby the T2-weighted anatomical image was not obtained due to scan time constraints. Further, the DWI parameters acquired at the first pregnancy scan differed from the sequence collected at subsequent timepoints due to the sequences still being in the testing phase at that time. Hence, the DWI data for the first pregnancy scan was excluded. All MR images were visually inspected for artifacts prior to processing.

2.3 MRI Data Processing

Structural data processing. The T1-weighted and T2-weighted anatomical images where automatically processed with the longitudinal stream (Reuter et al., 2012) in FreeSurfer (http://surfer.nmr.mgh.harvard.edu/). Specifically, an unbiased within-subject template space and image is created using robust, inverse consistent registration (Reuter et al., 2010). Several processing steps, such as skull stripping, Talairach transforms, atlas registration as well as spherical surface maps and parcellations are then initialized with common information from the within-subject template, significantly increasing reliability and statistical power in a longitudinal setting (Reuter et al., 2012). We visually checked the cortical reconstruction of each subject for inaccuracies and manually corrected major topological inaccuracies with control points and subsequently repeated the processing. Cortical thickness was calculated as the shortest distance between the GM/WM boundary and pial surface at each vertex across the cortical mantle, measured in millimeters (mm). In addition to vertex-based reconstruction, FreeSurfer automatically parcellated the cortex into 34 gyral-based regions-of-interest (ROIs) per hemisphere, according to the Desikan-Killiany atlas. For each of the 68 cortical parcellations, FreeSurfer calculates i) the average cortical thickness (in mm), ii) total cortical surface area of the pial (in mm^2), and iii) the various volume measures (in mm^3).

Functional data processing. Resting-state fMRI data was preprocessed using *fMRIPrep* 21.0.1 (Estaban et al., 2018; Esteban et al., 2019), which is based on *Nipype* 1.6.1 (Gorgolewski et al., 2011; Gorgolewski et al., 2018). For each of the BOLD runs, the following preprocessing was performed. First, a reference volume and its skull-stripped version were generated using a custom methodology of *fMRIPrep*. Head-motion parameters with respect to the BOLD reference (transformation matrices, and six corresponding rotation and translation parameters) are estimated before any spatiotemporal filtering using mcflirt (FSL

6.0.5.1:57b01774, (Jenkinson et al., 2002). BOLD runs were slice-time corrected to 0.971s (0.5 of slice acquisition range 0s-1.94s) using 3dTshift from AFNI (Cox & Hyde, 1997). The BOLD time-series (including slice-timing correction when applied) were resampled onto their original, native space by applying the transforms to correct for head-motion. These resampled BOLD time-series will be referred to as *preprocessed BOLD in original space*, or just *preprocessed BOLD*. The BOLD reference was then co-registered to the T1w reference using bbregister (FreeSurfer) which implements boundary-based registration (Greve & Fischl, 2009). Co-registration was configured with six degrees of freedom. Several confounding time-series were calculated based on the *preprocessed BOLD*: framewise displacement (FD), DVARS and three region-wise global signals. FD was computed using two formulations following Power (absolute sum of relative motions; Power et al., 2014) and Jenkinson (relative root mean square displacement between affines, Jenkinson et al. (2002)). FD and DVARS are calculated for each functional run, both using their implementations in *Nipype* (following the definitions by Power et al. 2014). The three global signals are extracted within the CSF, the WM, and the whole-brain masks. Additionally, a set of physiological regressors were extracted to allow for component-based noise correction (*CompCor*, Behzadi et al., 2007). Principal components are estimated after high-pass filtering the *preprocessed BOLD* time-series (using a discrete cosine filter with 128s cut-off) for the two *CompCor* variants: temporal (tCompCor) and anatomical (aCompCor). tCompCor components are then calculated from the top 2% variable voxels within the brain mask. For aCompCor, three probabilistic masks (CSF, WM, and combined CSF+WM) are generated in anatomical space. The implementation differs from that of Behzadi et al. in that instead of eroding the masks by 2 pixels on BOLD space, the aCompCor masks are subtracted a mask of pixels that likely contain a volume fraction of GM. This mask is obtained by dilating a

GM mask extracted from the FreeSurfer's *aseg* segmentation, and it ensures components are not extracted from voxels containing a minimal fraction of GM. Finally, these masks are resampled into BOLD space and binarized by thresholding at 0.99 (as in the original implementation). Components are also calculated separately within the WM and CSF masks. For each CompCor decomposition, the *k* components with the largest singular values are retained, such that the retained components' time series are sufficient to explain 50 percent of variance across the nuisance mask (CSF, WM, combined, or temporal). The remaining components are dropped from consideration. The head-motion estimates calculated in the correction step were also placed within the corresponding confounds file. The confound time series derived from head motion estimates and global signals were expanded with the inclusion of temporal derivatives and quadratic terms for each (Satterthwaite et al., 2013). Frames that exceeded a threshold of 0.5 mm FD or 1.5 standardised DVARS were annotated as motion outliers. The BOLD time-series were resampled into standard space, generating a *preprocessed BOLD run in MNI152NLin2009cAsym space*. First, a reference volume and its skull-stripped version were generated using a custom methodology of *fMRIPrep*. The BOLD time-series were resampled onto the fsaverage surfaces (FreeSurfer reconstruction nomenclature). *Grayordinates files* (Glasser et al., 2013) containing 91k samples were also generated using the highest-resolution fsaverage as intermediate standardized surface space. All resamplings can be performed with *a single interpolation step* by composing all the pertinent transformations (i.e., head-motion transform matrices, susceptibility distortion correction when available, and co-registrations to anatomical and output spaces). Gridded (volumetric) resamplings were performed using antsApplyTransforms (ANTs), configured with Lanczos interpolation to minimize the smoothing effects of other kernels (Lanczos, 1964). Non-gridded (surface) resamplings were performed

using mri_vol2surf (FreeSurfer). Preprocessed surface space data were next denoised, bandpass filtered (0.008-0.1 Hz), and the high motion volumes dropped from each run. Denoising regressed out global signal, FD, Volterra-expanded series from the 6 movement measures (rotation and translation in 3 directions, lagged 6 times), and censoring for timepoints that were over 0.2mm FD. Finally, runs collected in the same session were concatenated, resulting in 8 sets of data (4 peripartum and 4 postpartum) ranging in total duration from 9.4 to 36.8 minutes. The Gordon cortical (Gordon et al., 2016) parcellation scheme was then applied before further analysis resulting in denoised timeseries from 300 regions across the cortex.

Personalized network assignment. Processed connectivity data were concatenated across all visits and cross-correlated to generate a single connectivity matrix. This matrix was then thresholded to retain the top parcel–parcel connectivity strengths for network assignment. Network assignments were made by applying the Infomap algorithm (Lancichinetti & Fortunato, 2009), weighing map edges by correlation strength. This process was repeated using the following density thresholds: 0.01, 0.05, 0.1, 0.15, 0.2, 0.25. The density threshold that resulted in network assignments that were most comparable to those found in adults was retained (i.e., 0.1).

Network coherence and modularity. We computed two global network metrics, coherence (within-network connectivity) and modularity (ratio of with-network connectivity to out-of-network connectivity). These metrics were computed across binned timepoints whereby we pooled data from the first and third visits (early pregnancy), the fourth and fifth visit (late pregnancy), and the sixth-ninth visits (postpartum). Network measures and 95% confidence intervals were then estimated using a bootstrapping approach, where 10-20 minutes of data were randomly selected from the pooled data for network measurement computation. This process was

repeated 10,000 to generate a distribution of values to estimate the true network coherence and modularity for each network and binned timepoint. Because previous precision mapping has shown that at least 20 minutes of data are needed for reliable estimates (Laumann et al., 2015), we present results from the binned timepoints as opposed to individual timepoints.

Diffusion data processing. The DWI data were processed using tools from FSL (v6.0) and MRtrix3 (S. M. Smith et al., 2004; Tournier et al., 2019). First, the raw diffusion data was first converted from DICOM to MIF format using MRtrix3's mrconvert function. Next, the DWIs were denoised using dwidenoise, which has been shown to improve the subsequent estimation of diffusion parameters and fiber orientation distributions (Cordero-Grande et al., 2019; Veraart et al., 2016). FSL's TOPUP program was used to correct for distortions in the acquired diffusion-weighted images (which is critical for anatomically accurate tractography) (Andersson et al., 2003). MRtrix3's dwifslpreproc program was used to implement both TOPUP and FSL's eddy tool, which corrects for motion and eddy current artifacts including outlier replacement (Andersson et al., 2016; Andersson & Sotiropoulos, 2016). The T1w anatomical image was affine registered to the distortion-corrected b0 image using FSL's flirt program. With this transformation, the FreeSurfer-derived tissue masks were sampled to a subject's native DWI-space for use in anatomically-constrained tractography.

We first performed whole-brain streamline tractography to construct the subject's whole-brain white matter connectome at each timepoint. We used a custom, publicly-available pipeline (https://github.com/conradbn/DWI_Tractography) that was written in Python and built from the MRtrix3 software package (Tournier et al., 2019). The preprocessed DWI data were first used to fit a tensor model and derive FA and MD maps. To begin the tractography process, the same DWI data were passed to an unsupervised method for estimating single-fiber response functions

for WM, GM, and CSF (Aerts et al., 2019). Multi-shell, multi-tissue constrained spherical deconvolution was performed to obtain WM fiber orientation distributions (FODs) as well as for the GM and CSF compartments in all voxels (Jeurissen et al., 2014). The FOD maps were then corrected for intensity inhomogeneities and bias fields (Raffelt et al., 2017). Probabilistic tracking was employed to construct a whole-brain tractogram via the tckgen command and the "iFOD2" algorithm (Tournier et al., 2010). We generated 20 million streamlines which were randomly seeded and terminated at the GM/WM interface as delineated by the FreeSurfer Longitudinal pipeline segmentation files, in a method known as anatomically-constrained tractography (ACT) (R. E. Smith et al., 2012). ACT helps improve the biological validity of streamlines by ensuring that a streamline begins and ends (i.e., "synapses") at some GM structure. Finally, we used the "spherical-deconvolution informed filtering of tractograms" method (SIFT2), to correct for known biases in tractography by assigning a cross-sectional area weight to each streamline (Smith et al., 2015). SIFT2 provides a weighted streamline reconstruction that optimally fits the underlying CSD model at each voxel, effectively down-weighting false-positive streamlines. One can then sum the resulting weights of streamlines connecting any two brain regions to provide a measure proportional to the total cross-sectional area of WM fibers between the regions, i.e., a physically interpretable, quantitative measure of structural connectivity (Smith et al., 2020).

To determine the subject-specific white matter networks, we first performed a series of transformations to bring the subject-specific network parcellation into the native DWI space of the first session, which served as the reference space for the network parcellation. Each timepoint's DWI-space anatomical image was then registered to the first session's anatomical image, and the inverse transformation was applied to the parcellation image using nearest

neighbor interpolation. This resulted in the subject-specific GM network masks in DWI-space. For each network, we used MRtrix3's tckedit command to find the subset of streamlines that terminated in network mask at both ends, yielding a reconstruction of the WM fibers connecting the regions of each network. The tcksample command was then used to find the mean FA and mean MD across the volume occupied by each WM network.

After the study's completion, we discovered an issue with the b-value = 2500 scan (acquired in a separate sequence from the b-value = 500/1500) such that the sequence had been automatically split into two "packages" in four of eight sessions (i.e., scan length doubled and only half of slices acquired at each volume). This was due to an interaction with the prescribed scan parameters and slightly different head orientation/slice positioning from scan to scan. Though the data, resulting FA/MD maps, and tractography looked qualitatively normal, out of an abundance of caution we chose to analyze FA and MD using only the b-value = 500/1500 preprocessed data. These data, while not optimal for high-angular resolution tractography, are sufficient for reliable estimation of FA and MD (Chung et al., 2013; Soares et al., 2013). Further, the last postpartum timepoint (106 weeks gestation) had high absolute motion (0.85) (i.e., head moved from the most from beginning to end), but not relative motion (0.42) (volume-to-volume). Given that head motion is associated with changes in FA and MD values (Yendiki et al., 2014), we excluded the last postpartum timepoint from the diffusion analyses.

2.4 Data Analytical Plan

First, to examine morphometric changes, piecewise regression plots (i.e., segment one consists of the first scan in pregnancy [8 weeks] until the last pregnancy scan [37 weeks] and segment two from the last pregnancy scan until the final postpartum scan [106 weeks]) were generated for all volume estimates, as well as constituent measures in volume including mean

cortical thickness and surface area. Percent change was computed using the first and last scan from both segments described above. Second, to examine functional connectivity changes, stacked line plots were generated to depict changes from early to late pregnancy and from late pregnancy to postpartum across all networks for mean network coherence and mean network modularity, and percent changes were computed across the three binned timepoints for both metrics. Third, to examine structural connectivity changes, an identical approach to examine morphometric changes were used to examine FA and MD values for all networks and percent change was computed across pregnancy and from pregnancy to postpartum.

CHAPTER III

Results

3.1 Morphometric Results

Analysis of morphometric changes revealed that from 8 weeks gestation through term, total brain volume decreased by 3.4%, total gray matter volume decreased by 4.3%, total cortical volume decreased by 5.0%, total subcortical volume decreased by 2.5%, and total white matter volume decreased by 2.3%. In the postpartum period, total brain volume increased by 3.6%, total gray matter volume increased by 4.6%, total cortical volume increased by 5.7%, total subcortical volume increased by 3.1%, and total white matter volumes increased by 2.1%. In contrast, total ventricular volume increased by 7.5% from 8 weeks gestation through term and decreased by 9.2% in the postpartum period (See Figure 1).

Total surface area and mean cortical thickness also decreased from 8 weeks gestation through term by 2.1% and 2.5% respectively, followed by an increase of 2.7% and 2.2%, respectively, in the postpartum period (See Figure 1).

See Table 1 for piecewise regression results for changes in volume estimates, as well as changes in mean cortical thickness and surface area as a function of gestational age during pregnancy and in the postpartum period.

3.2 Functional Connectivity Results

For analysis of functional connectivity, network coherence and network modularity were computed across binned timepoints whereby we pooled data from the first and third visits (early pregnancy), the fourth and fifth visit (late pregnancy), and the sixth-ninth visits (postpartum)

because past precision mapping work has shown that at least 20 minutes of data are needed for computing reliable estimates (Laumann et al., 2015). Results revealed that there was a 8.7-25.3% increase in network coherence across networks during pregnancy. Exceptions include the somatomotor mouth network, which exhibited a 3.6% decrease. For the postpartum period, there was an increase in network coherence followed by a further 10.2-48.6% increase across networks in the postpartum period, with the exception of attention and visual, default mode and fronto-parietal, and auditory networks, which decreased by 1.7%, 5.5%, 1.7% respectively (See Figure 2). Mean network modularity primarily decreased by 1.3-33.9% across networks during pregnancy and mostly plateaued in the postpartum period (See Figure 3).

Further, we examined the overlap of bootstrapped 95% confidence intervals across binned timepoints to investigate whether differences were best explained by chance. Non-overlapping 95% CI are interpreted to be meaningful changes in connectivity over time whereas overlapping CI are interpreted as potentially chance differences. Using this framework, we found meaningful changes in mean network coherence for all networks except the somatomotor mouth network. Changes in mean network modularity were meaningful for auditory and somatomotor mouth networks. See Figures 4-5 for confidence interval plots and Table 2 for the confidence interval values.

3.3 Structural Connectivity Results

Analysis of structural connectivity revealed that across pregnancy, FA values increased for auditory, cingulo-opercular and dorsal attention, right visual lateral, somatomotor hand, and somatomotor mouth network tracts; and decreased for default mode and fronto-parietal, and attention and visual network tracts. In the postpartum period, FA values increased for cingulo-opercular and dorsal attention, default mode and fronto-parietal, attention and visual, and

somatomotor hand network tracts; decreased for the auditory network tract; and remained relatively stable for right lateral visual and somatomotor mouth network tracts (See Figure 6).

Further, analysis of mean diffusivity revealed homogenous results such that MD values increased during pregnancy and decreased in the postpartum period for all network tracts (See Figure 7).

See Tables 3 and 4, respectively, for piecewise regression results for changes in FA and MD as a function of gestational age during pregnancy and in the postpartum period.

CHAPTER IV

Discussion

In a proof-of-concept study of multimodal brain changes in a single individual who completed repeated MRI scans during pregnancy and in the postpartum period, we characterized morphometric changes, as well as changes in functional and structural connectivity using a custom subject-specific atlas. In line with the limited past non-human and human research on structural changes in the peripartum period (Cárdenas et al., 2020), we found decreases in total brain, total gray (including subordinate measures such as, total cortical and subcortical volume, total surface area, and mean cortical thickness), and total white matter volume estimates across pregnancy, followed by increases in the postpartum period. Further, consistent with research from Oatridge et al. (2002) we found an inverse trend for ventricular volume: increases across pregnancy and decreases in the postpartum period. Given the evidence that cerebrospinal fluid increases during pregnancy, it is possible that it may push against the brain, thereby contributing to the decreases in brain volume estimates and increase in ventricular volume during pregnancy (Andersson-Hall et al., 2021). Notably, unlike studies suggesting that volume reductions persist in the postpartum period (Hoekzema et al., 2017; Martínez-García et al., 2021), this study's results were similar to ones that found an increase in volume estimates in the postpartum period (Kim et al., 2010).

Analysis of functional connectivity revealed heterogeneity in changes in mean network coherence and network modularity. There were mainly increases in network coherence suggesting in increase in intranetwork connectivity across pregnancy as well as in the postpartum

period. Further, mean network modularity primarily decreased across pregnancy and mostly plateaued in the postpartum period. However, the large confidence intervals limit our confidence in whether this pattern is replicable. These findings extend past EEG and fNIRS studies that examined changes in brain activity during pregnancy (Raz, 2014; Roos et al., 2011) and suggest that the brain may be undergoing more global reorganization of networks in the peripartum period.

Further, analysis of structural connectivity revealed that FA values increased across pregnancy and subsequently plateaued in the postpartum period, potentially indicating changes in factors that are thought to contribute to changes in FA such as, fiber density, axonal diameter, and myelination in white matter tracts during pregnancy. In contrast, there was a decrease in MD values across pregnancy followed by a plateau in the postpartum period. This suggests that average molecular motion, independent of tissue directionality decreased across pregnancy for all network tracts.

The findings from this study underscores the need for further investigation into neurobiological mechanisms of change in the peripartum period. Pregnancy is a period marked by dramatic hormone changes. For example, progesterone and estrogen levels rise during pregnancy to support fetal development and drop after birth (Magon & Kumar, 2012). Similarly, cortisol level increases during pregnancy to ensure development of vital organs and the central nervous system (Murphy & Clifton, 2003), and typically declines quickly to baseline level postbirth (Thompson & Trevathan, 2008). In other contexts, changes in hormone levels are linked to structural and functional changes in the human brain. For instance, changes in sex steroid hormones during puberty is associated with alterations in gray and white matter volume (Peper et al., 2011). Further, during menopause, estrogen levels decline rapidly, accompanied by

reductions in gray matter volume (Kim et al., 2018). Causal evidence of the link between hormones and brain volume are supported in work from patients with Cushing's syndrome, a disorder characterized by hypercortisolism. Specifically, a study examining 38 patients with Cushing's syndrome found that loss of measured brain volume that was very significantly reversed at 40 months after achieving eucortisolism (i.e., cortisol level within the normal range) (Bourdeau et al., 2002). Another biological system that undergoes changes during pregnancy is the immune system, as it becomes suppressed to reduce attacks on the fetus, a foreign body (Munoz-Suano et al., 2011). For instance, levels of proinflammatory cytokines, mediators of immune responses that promote inflammation, increase during pregnancy (Bränn et al., 2017). Increased inflammation was found to be associated with increased amygdala activity to socially threatening images in a sample of non-pregnant adults (Inagaki et al., 2012). Thus, to better understand if these brain changes in the peripartum period may be consequences of other biological changes, it is necessary for future work to investigate changes in hormone and inflammation levels across pregnancy and in the postpartum period, and examine associations with changes in brain metrics.

Along with examining predictors of change, it is critical to also examine potential functional consequences of these brain changes. Gray matter volume reductions have been associated with declines in cognitive performance in studies of adult aging (Ramanoël et al., 2018). Thus, it is possible that the decline in brain volume estimates may be driving the cognitive changes during pregnancy and in the postpartum period including memory disturbances, trouble concentrating, and absentmindedness (Henry & Rendell, 2007). The brain changes in the peripartum period may also confer increased risk for mood disorders as changes in sex steroid hormones post-delivery is associated with symptoms of depression (Trifu et al., 2019).

Examining trajectories of hormone changes and their associations with brain changes in the peripartum period would help shed light on potential timing and targets of interventions aimed at promoting maternal mental health.

This study has five limitations. First, assessment of brain changes began in early pregnancy and the study did not capture the full period from conception to birth. Second, data was collected at inconsistent intervals across pregnancy and postpartum, with a large period postpartum missing due to the COVID-19 pandemic shutdowns and thus lack of data may have influenced the ability to detect the shape of change. Third, while brain size is being examined using volume estimates, it is unclear what might be driving the changes in measurement (i.e., whether the brain is undergoing cortical loss or cortical rearrangement/compression during pregnancy, either of which could result in the appearance of volume decreases). Fourth, we are not able to provide information about the potential causes and effects of observed brain changes as sleep, mood, cognition, hormonal, and inflammatory changes were not examined. Lastly, this work evaluated brain changes in a single individual and thus these changes may not be found in other individuals.

To conclude, the present study characterized brain plasticity in a single individual and provides support for the existence of morphometric, and functional and structural connectivity changes in the peripartum period. The findings motivate efforts to further expand this important area of research by examining changes in a larger sample and investigating predictors and potential functional consequences of these changes.

References

Aerts, H., Dhollander, T., & Marinazzo, D. (2019). *Evaluating the performance of 3-tissue constrained spherical deconvolution pipelines for within-tumor tractography* [Preprint]. Neuroscience. https://doi.org/10.1101/629873

Andersson, J. L. R., Graham, M. S., Zsoldos, E., & Sotiropoulos, S. N. (2016). Incorporating outlier detection and replacement into a non-parametric framework for movement and distortion correction of diffusion MR images. *NeuroImage*, *141*, 556–572. https://doi.org/10.1016/j.neuroimage.2016.06.058

Andersson, J. L. R., Skare, S., & Ashburner, J. (2003). How to correct susceptibility distortions in spin-echo echo-planar images: Application to diffusion tensor imaging. *NeuroImage*, *20*(2), 870–888. https://doi.org/10.1016/S1053-8119(03)00336-7

Andersson, J. L. R., & Sotiropoulos, S. N. (2016). An integrated approach to correction for off-resonance effects and subject movement in diffusion MR imaging. *NeuroImage*, *125*, 1063–1078. https://doi.org/10.1016/j.neuroimage.2015.10.019

Andersson-Hall, U., Svedin, P., Mallard, C., Blennow, K., Zetterberg, H., & Holmäng, A. (2021). Growth differentiation factor 15 increases in both cerebrospinal fluid and serum during pregnancy. *PLOS ONE*, *16*(5), e0248980. https://doi.org/10.1371/journal.pone.0248980

Behzadi, Y., Restom, K., Liau, J., & Liu, T. T. (2007). A component based noise correction method (CompCor) for BOLD and perfusion based fMRI. *NeuroImage*, *37*(1), 90–101. https://doi.org/10.1016/j.neuroimage.2007.04.042

Boeldt, D. S., & Bird, I. M. (2017). Vascular adaptation in pregnancy and endothelial dysfunction in preeclampsia. *Journal of Endocrinology*, *232*(1), R27–R44. https://doi.org/10.1530/JOE-16-0340

Bourdeau, I., Cordeau, M.-P., Lair, M. B., Lesage, J., Lafontaine, L., & Lacroix, A. (2002). Loss of Brain Volume in Endogenous Cushing's Syndrome and Its Reversibility after Correction of Hypercortisolism. *The Journal of Clinical Endocrinology & Metabolism*, *87*(5), 1949–1954.

Bränn, E., Papadopoulos, F., Fransson, E., White, R., Edvinsson, Å., Hellgren, C., Kamali-Moghaddam, M., Boström, A., Schiöth, H. B., Sundström-Poromaa, I., & Skalkidou, A. (2017). Inflammatory markers in late pregnancy in association with postpartum depression—A nested case-control study. *Psychoneuroendocrinology*, *79*, 146–159. https://doi.org/10.1016/j.psyneuen.2017.02.029

Brett, M., & Baxendale, S. (2001). Motherhood and memory: A review. *Psychoneuroendocrinology*, *26*(4), 339–362. https://doi.org/10.1016/S0306-4530(01)00003-8

Brunton, P. J., & Russell, J. A. (2008). The expectant brain: Adapting for motherhood. *Nature Reviews Neuroscience*, *9*(1), 11–25. https://doi.org/10.1038/nrn2280

Cárdenas, E. F., Kujawa, A., & Humphreys, K. L. (2020). Neurobiological changes during the peripartum period: Implications for health and behavior. *Social Cognitive and Affective Neuroscience*, *15*(10), 1097–1110. https://doi.org/10.1093/scan/nsz091

Casey, P., Huntsdale, C., Angus, G., & Janes, C. (1999). Memory in pregnancy. II: Implicit, incidental, explicit, semantic, short-term, working and prospective memory in

primigravid, multigravid and postpartum women. *Journal of Psychosomatic Obstetrics & Gynecology*, *20*(3), 158–164. https://doi.org/10.3109/01674829909075590

Cordero-Grande, L., Christiaens, D., Hutter, J., Price, A. N., & Hajnal, J. V. (2019). Complex diffusion-weighted image estimation via matrix recovery under general noise models. *NeuroImage*, *200*, 391–404. https://doi.org/10.1016/j.neuroimage.2019.06.039

Cox, R. W., & Hyde, J. S. (1997). Software tools for analysis and visualization of fMRI data. *NMR in Biomedicine*, *10*(4–5), 171–178. https://doi.org/10.1002/(SICI)1099-1492(199706/08)10:4/5<171::AID-NBM453>3.0.CO;2-L

Estaban, O., Blair, R., Markiewicz, C. J., Berleant, S. L., Moodie, C., Ma, F., Isik, A. I., Erramuzpe, A., Kent, M., & James, D. (2018). Fmriprep. *Software*.

Esteban, O., Markiewicz, C. J., Blair, R. W., Moodie, C. A., Isik, A. I., Erramuzpe, A., Kent, J. D., Goncalves, M., DuPre, E., Snyder, M., Oya, H., Ghosh, S. S., Wright, J., Durnez, J., Poldrack, R. A., & Gorgolewski, K. J. (2019). fMRIPrep: A robust preprocessing pipeline for functional MRI. *Nature Methods*, *16*(1), 111–116. https://doi.org/10.1038/s41592-018-0235-4

Glasser, M. F., Sotiropoulos, S. N., Wilson, J. A., Coalson, T. S., Fischl, B., Andersson, J. L., Xu, J., Jbabdi, S., Webster, M., Polimeni, J. R., Van Essen, D. C., & Jenkinson, M. (2013). The minimal preprocessing pipelines for the Human Connectome Project. *NeuroImage*, *80*, 105–124. https://doi.org/10.1016/j.neuroimage.2013.04.127

Gordon, E. M., Laumann, T. O., Adeyemo, B., Huckins, J. F., Kelley, W. M., & Petersen, S. E. (2016). Generation and Evaluation of a Cortical Area Parcellation from Resting-State Correlations. *Cerebral Cortex*, *26*(1), 288–303. https://doi.org/10.1093/cercor/bhu239

Gorgolewski, K., Burns, C. D., Madison, C., Clark, D., Halchenko, Y. O., Waskom, M. L., & Ghosh, S. S. (2011). Nipype: A Flexible, Lightweight and Extensible Neuroimaging Data Processing Framework in Python. *Frontiers in Neuroinformatics*, *5*. https://doi.org/10.3389/fninf.2011.00013

Gorgolewski, K. J., Nichols, T., Kennedy, D. N., Poline, J.-B., & Poldrack, R. A. (2018). Making replication prestigious. *Behavioral and Brain Sciences*, *41*, e131. https://doi.org/10.1017/S0140525X18000663

Greve, D. N., & Fischl, B. (2009). Accurate and robust brain image alignment using boundary-based registration. *NeuroImage*, *48*(1), 63–72. https://doi.org/10.1016/j.neuroimage.2009.06.060

Henry, J. D., & Rendell, P. G. (2007). A review of the impact of pregnancy on memory function. *Journal of Clinical and Experimental Neuropsychology*, *29*(8), 793–803. https://doi.org/10.1080/13803390701612209

Hillerer, K. M., Jacobs, V. R., Fischer, T., & Aigner, L. (2014a). The maternal brain: An organ with peripartal plasticity. *Neural Plasticity*, *2014*. https://doi.org/10.1155/2014/574159

Hillerer, K. M., Jacobs, V. R., Fischer, T., & Aigner, L. (2014b). The Maternal Brain: An Organ with Peripartal Plasticity. *Neural Plasticity*, *2014*, 1–20. https://doi.org/10.1155/2014/574159

Hoekzema, E., Barba-Müller, E., Pozzobon, C., Picado, M., Lucco, F., García-García, D., Soliva, J. C., Tobeña, A., Desco, M., Crone, E. A., Ballesteros, A., Carmona, S., & Vilarroya, O. (2017). Pregnancy leads to long-lasting changes in human brain structure. *Nature Neuroscience*, *20*(2), 287–296. https://doi.org/10.1038/nn.4458

Inagaki, T. K., Muscatell, K. A., Irwin, M. R., Cole, S. W., & Eisenberger, N. I. (2012). Inflammation selectively enhances amygdala activity to socially threatening images. *NeuroImage*, *59*(4), 3222–3226. https://doi.org/10.1016/j.neuroimage.2011.10.090

Jenkinson, M., Bannister, P., Brady, M., & Smith, S. (2002). Improved Optimization for the Robust and Accurate Linear Registration and Motion Correction of Brain Images. *NeuroImage*, *17*(2), 825–841. https://doi.org/10.1006/nimg.2002.1132

Jeurissen, B., Tournier, J.-D., Dhollander, T., Connelly, A., & Sijbers, J. (2014). Multi-tissue constrained spherical deconvolution for improved analysis of multi-shell diffusion MRI data. *NeuroImage*, *103*, 411–426. https://doi.org/10.1016/j.neuroimage.2014.07.061

Kim, G.-W., Park, K., & Jeong, G.-W. (2018). Effects of Sex Hormones and Age on Brain Volume in Post-Menopausal Women. *The Journal of Sexual Medicine*, *15*(5), 662–670. https://doi.org/10.1016/j.jsxm.2018.03.006

Kim, P., Leckman, J. F., Mayes, L. C., Feldman, R., Wang, X., & Swain, J. E. (2010a). The plasticity of human maternal brain: Longitudinal changes in brain anatomy during the early postpartum period. *Behavioral Neuroscience*, *124*(5), 695–700. https://doi.org/10.1037/a0020884

Kim, P., Leckman, J. F., Mayes, L. C., Feldman, R., Wang, X., & Swain, J. E. (2010b). The plasticity of human maternal brain: Longitudinal changes in brain anatomy during the early postpartum period. *Behavioral Neuroscience*, *124*(5), 695–700. https://doi.org/10.1037/a0020884

Lancichinetti, A., & Fortunato, S. (2009). Community detection algorithms: A comparative analysis. *Physical Review E*, *80*(5), 056117. https://doi.org/10.1103/PhysRevE.80.056117

Lanczos, C. (1964). Evaluation of noisy data. *Journal of the Society for Industrial and Applied Mathematics*, *1*(1), 76–85.

Laumann, T. O., Gordon, E. M., Adeyemo, B., Snyder, A. Z., Joo, S. J., Chen, M.-Y., Gilmore, A. W., McDermott, K. B., Nelson, S. M., Dosenbach, N. U. F., Schlaggar, B. L., Mumford, J. A., Poldrack, R. A., & Petersen, S. E. (2015). Functional System and Areal Organization of a Highly Sampled Individual Human Brain. *Neuron*, *87*(3), 657–670. https://doi.org/10.1016/j.neuron.2015.06.037

Levine, D. (2013). Timing of MRI in pregnancy, repeat exams, access, and physician qualifications. *Seminars in Perinatology*, *37*(5), 340–344. https://doi.org/10.1053/j.semperi.2013.06.011

Magon, N., & Kumar, P. (2012). Hormones in pregnancy. *Nigerian Medical Journal*, *53*(4), 179. https://doi.org/10.4103/0300-1652.107549

Markon, K. E., Brunette, C. A., Whitney, B. M., & O'Hara, M. W. (2021). Mood during pregnancy: Trends, structure, and invariance by gestational day. *Journal of Psychiatric Research*, *140*, 260–266. https://doi.org/10.1016/j.jpsychires.2021.06.006

Martínez-García, M., Paternina-Die, M., Barba-Müller, E., Martín de Blas, D., Beumala, L., Cortizo, R., Pozzobon, C., Marcos-Vidal, L., Fernández-Pena, A., Picado, M., Belmonte-Padilla, E., Massó-Rodriguez, A., Ballesteros, A., Desco, M., Vilarroya, Ó., Hoekzema, E., & Carmona, S. (2021). Do Pregnancy-Induced Brain Changes Reverse? The Brain of a Mother Six Years after Parturition. *Brain Sciences*, *11*(2), 168. https://doi.org/10.3390/brainsci11020168

Munoz-Suano, A., Hamilton, A. B., & Betz, A. G. (2011). Gimme shelter: The immune system during pregnancy: The Immunology of Pregnancy. *Immunological Reviews*, *241*(1), 20–38. https://doi.org/10.1111/j.1600-065X.2011.01002.x

Murphy, V. E., & Clifton, V. L. (2003). Alterations in Human Placental 11β-hydroxysteroid Dehydrogenase Type 1 and 2 with Gestational Age and Labour. *Placenta*, *24*(7), 739–744. https://doi.org/10.1016/S0143-4004(03)00103-6

Newham, J. J., & Martin, C. R. (2013). Measuring fluctuations in maternal well-being and mood across pregnancy. *Journal of Reproductive and Infant Psychology*, *31*(5), 531–540. https://doi.org/10.1080/02646838.2013.834040

Oatridge, A., Holdcroft, A., Saeed, N., Hajnal, J. V., Puri, B. K., Fusi, L., & Bydder, G. M. (2002). *Change in Brain Size during and after Pregnancy: Study in Healthy Women and Women with Preeclampsia*. *23*(1), 19–26.

Patenaude, Y., Pugash, D., Lim, K., Morin, L., Lim, K., Bly, S., Butt, K., Cargill, Y., Davies, G., Denis, N., Hazlitt, G., Morin, L., Naud, K., Ouellet, A., & Salem, S. (2014). The Use of Magnetic Resonance Imaging in the Obstetric Patient. *Journal of Obstetrics and Gynaecology Canada*, *36*(4), 349–355. https://doi.org/10.1016/S1701-2163(15)30612-5

Peper, J. S., van den Heuvel, M. P., Mandl, R. C. W., Pol, H. E. H., & van Honk, J. (2011). Sex steroids and connectivity in the human brain: A review of neuroimaging studies. *Psychoneuroendocrinology*, *36*(8), 1101–1113. https://doi.org/10.1016/j.psyneuen.2011.05.004

Power, J. D., Schlaggar, B. L., & Petersen, S. E. (2014). Studying Brain Organization via Spontaneous fMRI Signal. *Neuron*, *84*(4), 681–696. https://doi.org/10.1016/j.neuron.2014.09.007

Raffelt, D. A., Tournier, J.-D., Smith, R. E., Vaughan, D. N., Jackson, G., Ridgway, G. R., & Connelly, A. (2017). Investigating white matter fibre density and morphology using fixel-based analysis. *NeuroImage*, *144*, 58–73. https://doi.org/10.1016/j.neuroimage.2016.09.029

Ramanoël, S., Hoyau, E., Kauffmann, L., Renard, F., Pichat, C., Boudiaf, N., Krainik, A., Jaillard, A., & Baciu, M. (2018). Gray Matter Volume and Cognitive Performance During Normal Aging. A Voxel-Based Morphometry Study. *Frontiers in Aging Neuroscience*, *10*, 235. https://doi.org/10.3389/fnagi.2018.00235

Raz, S. (2014). Behavioral and neural correlates of cognitive–affective function during late pregnancy: An Event-Related Potentials Study. *Behavioural Brain Research*, *267*, 17–25. https://doi.org/10.1016/j.bbr.2014.03.021

Reuter, M., Rosas, H. D., & Fischl, B. (2010). Highly accurate inverse consistent registration: A robust approach. *NeuroImage*, *53*(4), 1181–1196. https://doi.org/10.1016/j.neuroimage.2010.07.020

Reuter, M., Schmansky, N. J., Rosas, H. D., & Fischl, B. (2012). Within-subject template estimation for unbiased longitudinal image analysis. *NeuroImage*, *61*(4), 1402–1418. https://doi.org/10.1016/j.neuroimage.2012.02.084

Roos, A., Robertson, F., Lochner, C., Vythilingum, B., & Stein, D. J. (2011). Altered prefrontal cortical function during processing of fear-relevant stimuli in pregnancy. *Behavioural Brain Research*, *222*(1), 200–205. https://doi.org/10.1016/j.bbr.2011.03.055

Satterthwaite, T. D., Elliott, M. A., Gerraty, R. T., Ruparel, K., Loughead, J., Calkins, M. E., Eickhoff, S. B., Hakonarson, H., Gur, R. C., Gur, R. E., & Wolf, D. H. (2013). An improved framework for confound regression and filtering for control of motion artifact

in the preprocessing of resting-state functional connectivity data. *NeuroImage*, *64*, 240–256. https://doi.org/10.1016/j.neuroimage.2012.08.052

Shagana, J. A., Dhanraj, M., Jain, A. R., & Nirosa, T. (2018). Physiological changes in pregnancy. *Drug Invention Today*, *10*(8), 5.

Smith, R. E., Tournier, J.-D., Calamante, F., & Connelly, A. (2012). Anatomically-constrained tractography: Improved diffusion MRI streamlines tractography through effective use of anatomical information. *NeuroImage*, *62*(3), 1924–1938. https://doi.org/10.1016/j.neuroimage.2012.06.005

Smith, R. E., Tournier, J.-D., Calamante, F., & Connelly, A. (2015). SIFT2: Enabling dense quantitative assessment of brain white matter connectivity using streamlines tractography. *NeuroImage*, *119*, 338–351. https://doi.org/10.1016/j.neuroimage.2015.06.092

Smith, R., Raffelt, D., Tournier, J.-D., & Connelly, A. (2020). *Quantitative streamlines tractography: Methods and inter-subject normalisation* [Preprint]. Open Science Framework. https://doi.org/10.31219/osf.io/c67kn

Smith, S. M., Jenkinson, M., Woolrich, M. W., Beckmann, C. F., Behrens, T. E. J., Johansen-Berg, H., Bannister, P. R., De Luca, M., Drobnjak, I., Flitney, D. E., Niazy, R. K., Saunders, J., Vickers, J., Zhang, Y., De Stefano, N., Brady, J. M., & Matthews, P. M. (2004). Advances in functional and structural MR image analysis and implementation as FSL. *NeuroImage*, *23*, S208–S219. https://doi.org/10.1016/j.neuroimage.2004.07.051

Soares, J. M., Marques, P., Alves, V., & Sousa, N. (2013). A hitchhiker's guide to diffusion tensor imaging. *Frontiers in Neuroscience*, *7*. https://doi.org/10.3389/fnins.2013.00031

Thompson, L. A., & Trevathan, W. R. (2008). Cortisol reactivity, maternal sensitivity, and learning in 3-month-old infants. *Infant Behavior and Development*, *31*(1), 92–106. https://doi.org/10.1016/j.infbeh.2007.07.007

Tocchio, S., Kline-Fath, B., Kanal, E., Schmithorst, V. J., & Panigrahy, A. (2015). MRI evaluation and safety in the developing brain. *Seminars in Perinatology*, *39*(2), 73–104. https://doi.org/10.1053/j.semperi.2015.01.002

Tournier, J.-D., Calamante, F., & Connelly, A. (2010). Improved probabilistic streamlines tractography by 2nd order integration over fibre orientation distributions. *Proceedings of the International Society for Magnetic Resonance in Medicine*, *1670*.

Tournier, J.-D., Smith, R., Raffelt, D., Tabbara, R., Dhollander, T., Pietsch, M., Christiaens, D., Jeurissen, B., Yeh, C.-H., & Connelly, A. (2019). MRtrix3: A fast, flexible and open software framework for medical image processing and visualisation. *NeuroImage*, *202*, 116137. https://doi.org/10.1016/j.neuroimage.2019.116137

Trifu, S., Vladuti, A., & Popescu, A. (2019). Neuroendocrine Aspects of Pregnancy and Postpartum Depression. *Acta Endocrinologica (Bucharest)*, *15*(3), 410–415. https://doi.org/10.4183/aeb.2019.410

Veraart, J., Novikov, D. S., Christiaens, D., Ades-aron, B., Sijbers, J., & Fieremans, E. (2016). Denoising of diffusion MRI using random matrix theory. *NeuroImage*, *142*, 394–406. https://doi.org/10.1016/j.neuroimage.2016.08.016

Wu, W., Lien, S., Chang, J., & Yang, S. (2014). Caffeine alters resting-state functional connectivity measured by blood oxygenation level-dependent MRI. *NMR in Biomedicine*, *27*(4), 444–452. https://doi.org/10.1002/nbm.3080

Yendiki, A., Koldewyn, K., Kakunoori, S., Kanwisher, N., & Fischl, B. (2014). Spurious group differences due to head motion in a diffusion MRI study. *NeuroImage*, *88*, 79–90. https://doi.org/10.1016/j.neuroimage.2013.11.027

Table 1

Regression Results for Changes in Volume and Constituent Measures in Volume as a Function of Gestational Age

Structural Metric	*β*	*SE*	*t*	*95% CI*	*p*	R^2
Total Brain Volume:						
Pregnancy	-0.98	0.10	-9.76	-1.31, -0.66	.002	0.96
Postpartum	0.89	0.26	3.45	0.07, 1.72	.041	0.73
Total Gray Matter Volume:						
Pregnancy	-1.00	0.06	-17.48	-1.18, -0.81	<.001	0.99
Postpartum	0.88	0.28	3.16	-0.01, 1.76	.051	0.69
Total Cortical Volume:						
Pregnancy	-0.99	0.07	-14.18	-1.22, -0.77	<.001	0.98
Postpartum	0.90	0.26	3.51	0.08, 1.71	.039	0.74
Total Subcortical Volume:						
Pregnancy	-0.96	0.17	-5.64	-1.50, -0.42	.011	0.89
Postpartum	0.89	0.26	3.42	0.06, 1.72	.042	0.73
Total White Matter Volume:						
Pregnancy	-0.91	0.24	-3.76	-1.68, -0.14	.033	0.77
Postpartum	0.89	0.27	3.29	0.03, 1.74	.046	0.71
Total Ventricular Volume:						
Pregnancy	0.97	0.13	7.50	0.56, 1.39	.005	0.93
Postpartum	-0.48	0.51	-0.95	-2.09, 1.13	.411	-0.02
Mean Cortical Thickness:						
Pregnancy	-0.94	0.20	-4.77	-1.57, -0.31	.017	0.84
Postpartum	0.74	0.39	1.89	-0.50, 1.98	0.16	0.39
Total Surface Area:						
Pregnancy	-0.96	0.15	-6.36	-1.45, -0.48	.008	0.91
Postpartum	0.88	0.27	3.21	0.01, 1.75	.049	0.70

Table 2

Mean Network Coherence and Modularity for Binned Timepoints

Network	Timepoint	Mean Network Coherence [95% CI]	Changes Found in Network Coherence	Mean Network Modularity [95% CI]	Changes Found in Network Modularity
Attention and Visual	Early Pregnancy	0.056 [0.053, 0.059]	LP > EP	1.290 [1.228, 1.343]	
	Late Pregnancy	0.068 [0.065, 0.072]		1.218 [1.165, 1.268]	
	Postpartum	0.067 [0.063, 0.072]		1.182 [1.114, 1.251]	
Auditory	Early Pregnancy	0.073 [0.067, 0.079]	LP > EP	1.751 [1.597, 1.883]	LP > EP
	Late Pregnancy	0.110 [0.103, 0.119]		2.071 [1.926, 2.200]	
	Postpartum	0.108 [0.097, 0.120]		2.212 [1.995, 2.426]	
Cingulo-Opercular and Dorsal Attention	Early Pregnancy	0.087 [0.084, 0.092]	LP > EP; PP > LP	2.125 [2.006, 2.217]	
	Late Pregnancy	0.095 [0.091, 0.100]		2.079 [1.976, 2.164]	
	Postpartum	0.105 [0.097, 0.113]		2.232 [2.082, 2.371]	
Default mode and Fronto-Parietal	Early Pregnancy	0.058 [0.056, 0.061]	LP > EP	1.355 [1.316, 1.386]	
	Late Pregnancy	0.067 [0.065, 0.070]		1.337 [1.300, 1.369]	
	Postpartum	0.063 [0.060, 0.067]		1.325 [1.273, 1.374]	
Right Lateral Visual	Early Pregnancy	0.060 [0.054, 0.066]	LP > EP; PP > LP	1.311 [1.182, 1.439]	
	Late Pregnancy	0.075 [0.069, 0.081]		1.243 [1.148, 1.339]	
	Postpartum	0.096 [0.087, 0.106]		1.254 [1.143, 1.368]	
Somatomotor Hand	Early Pregnancy	0.082 [0.078, 0.087]	LP > EP; PP > LP	1.712 [1.589, 1.821]	
	Late Pregnancy	0.092 [0.086, 0.098]		1.607 [1.495, 1.720]	
	Postpartum	0.122 [0.111, 0.134]		1.533 [1.417, 1.653]	
Somatomotor Mouth	Early Pregnancy	0.073 [0.067, 0.079]	PP > LP-	1.497 [1.351, 1.641]	LP < EP; PP > LP
	Late Pregnancy	0.070 [0.064, 0.077]		0.989 [0.901, 1.082]	
	Postpartum	0.104 [0.095, 0.114]		1.330 [1.212, 1.454]	

Note. EP = Early Pregnancy (8 and 10 weeks gestation). LP = Late Pregnancy (35 and 37 weeks gestation). PP = Postpartum (68, 76, 96, and 106 weeks gestation).

Table 3

Regression Results for Changes in Functional Anisotropy as a Function of Gestational Age

Network Tract	*β*	*SE*	*t*	*95% CI*	*p*	R^2
Attention and Visual:						
Pregnancy	-0.86	0.35	-2.44	-2.39, 0.66	.135	0.62
Postpartum	0.92	0.28	3.24	-0.30, 2.13	.084	0.76
Auditory:						
Pregnancy	-0.14	0.70	-0.21	-3.15, 2.87	.856	-0.47
Postpartum	-0.70	0.50	-1.40	-2.86, 1.45	.295	0.24
Cingulo-Opercular and Dorsal Attention:						
Pregnancy	0.13	0.70	0.19	-2.88, 3.15	.867	-0.47
Postpartum	0.85	0.37	2.27	-0.76, 2.46	.151	0.58
Default mode and Fronto-Parietal:						
Pregnancy	-0.94	0.24	-3.90	-1.98, 0.10	.060	0.83
Postpartum	0.75	0.47	1.58	-1.28, 2.77	.254	0.33
Right Lateral Visual:						
Pregnancy	0.72	0.49	1.47	-1.39, 2.83	.279	0.28
Postpartum	0.35	0.66	0.53	-2.50, 3.20	.649	-0.32
Somatomotor Hand:						
Pregnancy	0.91	0.30	3.08	-0.36, 2.18	.091	0.74
Postpartum	0.98	0.13	7.87	0.45, 1.52	.016	0.95
Somatomotor Mouth:						
Pregnancy	0.97	0.18	5.44	0.20, 1.73	.032	0.91
Postpartum	0.68	0.52	1.32	-1.54, 2.90	.317	0.20

Table 4

Regression Results for Changes in Mean Diffusivity as a Function of Gestational Age

Network Tract	*β*	*SE*	*t*	*95% CI*	*p*	R^2
Attention and Visual:						
Pregnancy	0.94	0.25	3.78	-0.13, 2.00	.064	0.82
Postpartum	-0.97	0.17	-5.63	-1.71, -0.23	.030	0.91
Auditory:						
Pregnancy	0.94	0.24	3.84	-0.11, 1.99	.062	0.82
Postpartum	-0.90	0.31	-2.94	-2.22, 0.42	.099	0.72
Cingulo-Opercular and Dorsal Attention:						
Pregnancy	0.99	0.09	11.61	0.62, 1.36	.007	0.98
Postpartum	-0.92	0.27	-3.43	-2.09, 0.24	.076	0.78
Default mode and Fronto-Parietal:						
Pregnancy	0.98	0.13	7.37	0.41, 1.56	.018	0.95
Postpartum	-0.93	0.25	-3.67	-2.03, 0.16	.067	0.81
Right Lateral Visual:						
Pregnancy	0.96	0.20	4.91	0.12, 1.80	.039	0.89
Postpartum	-0.97	0.18	-5.48	-1.73, -0.21	.032	0.91
Somatomotor Hand:						
Pregnancy	0.96	0.20	4.72	0.08, 1.83	.042	0.88
Postpartum	-0.91	0.29	-3.12	-2.17, 0.35	.089	0.74
Somatomotor Mouth:						
Pregnancy	0.97	0.17	5.70	0.23, 1.70	.029	0.91
Postpartum	-0.93	0.26	-3.52	-2.06, 0.21	.072	0.79

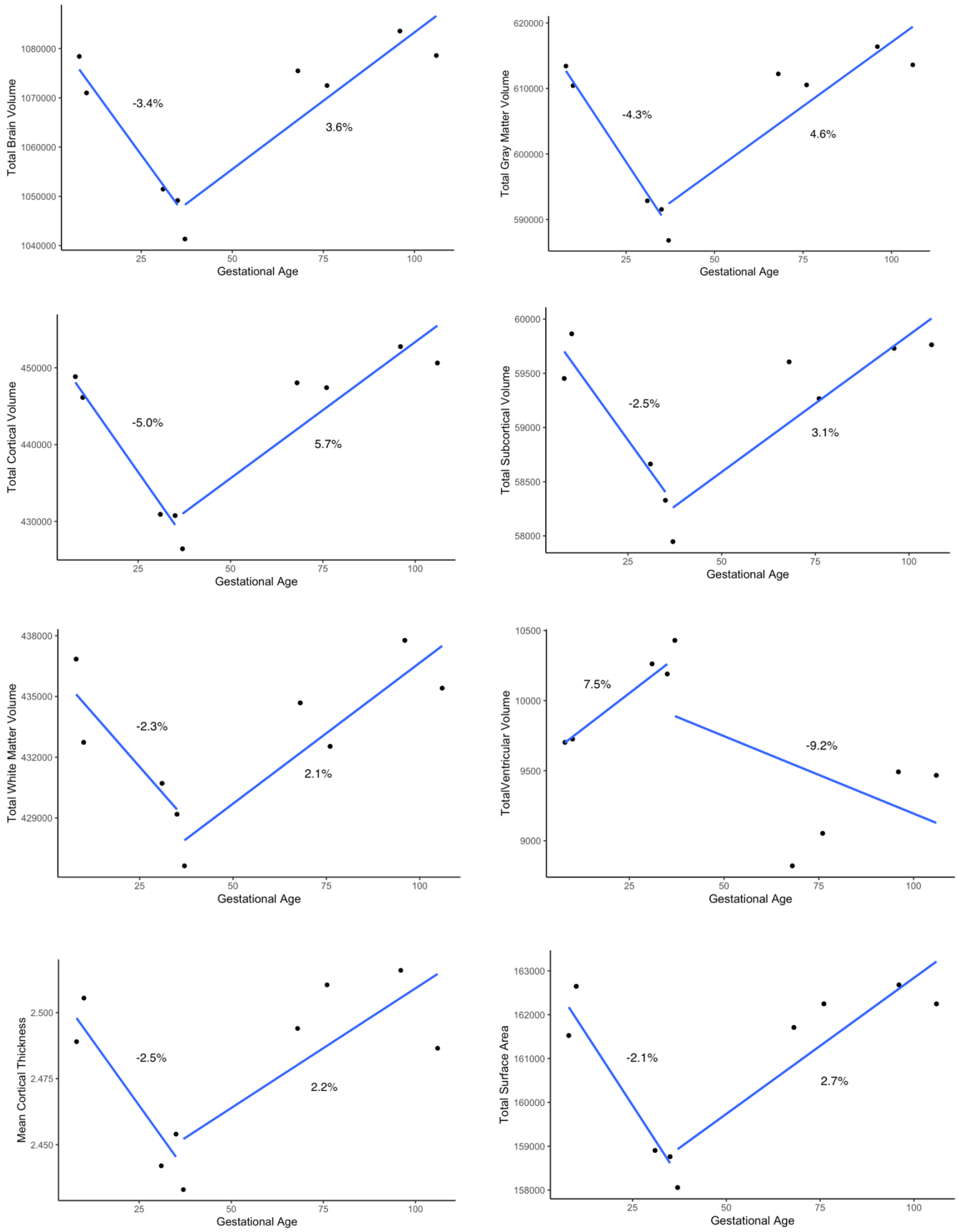

Figure 1. Morphometric Changes Across Gestational Age

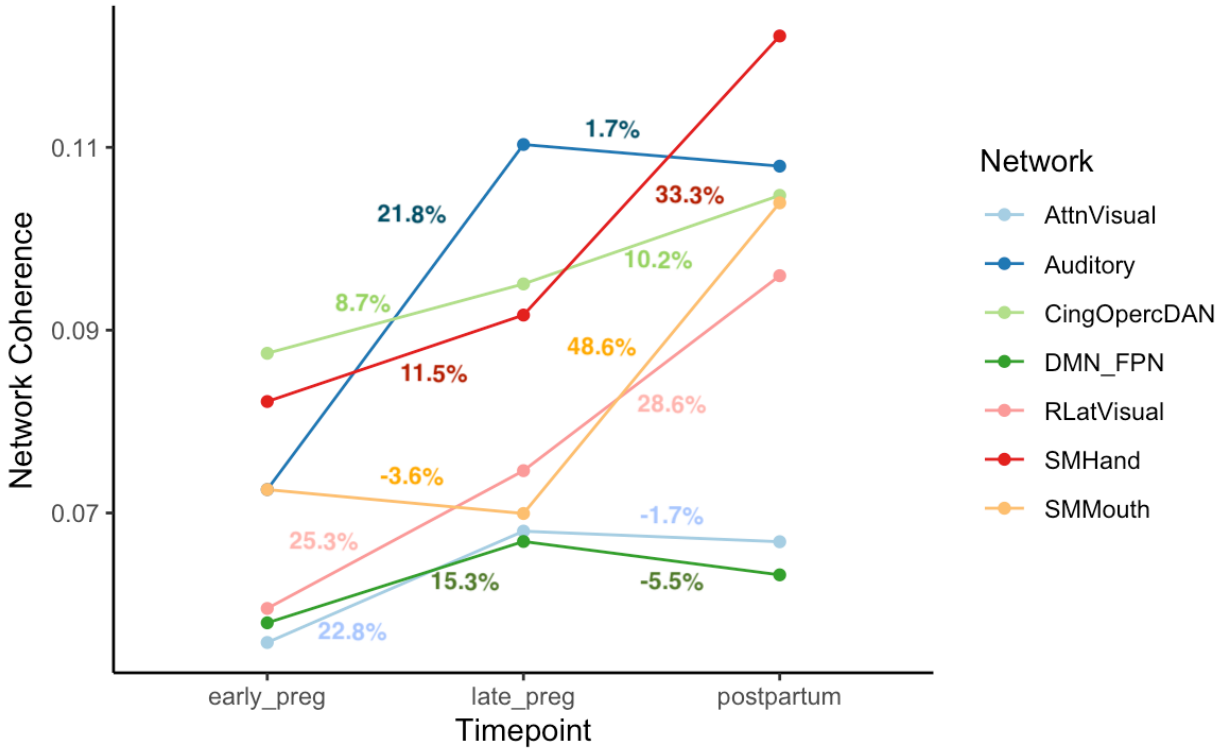

Figure 2. Changes in Mean Network Coherence Across Binned Timepoints

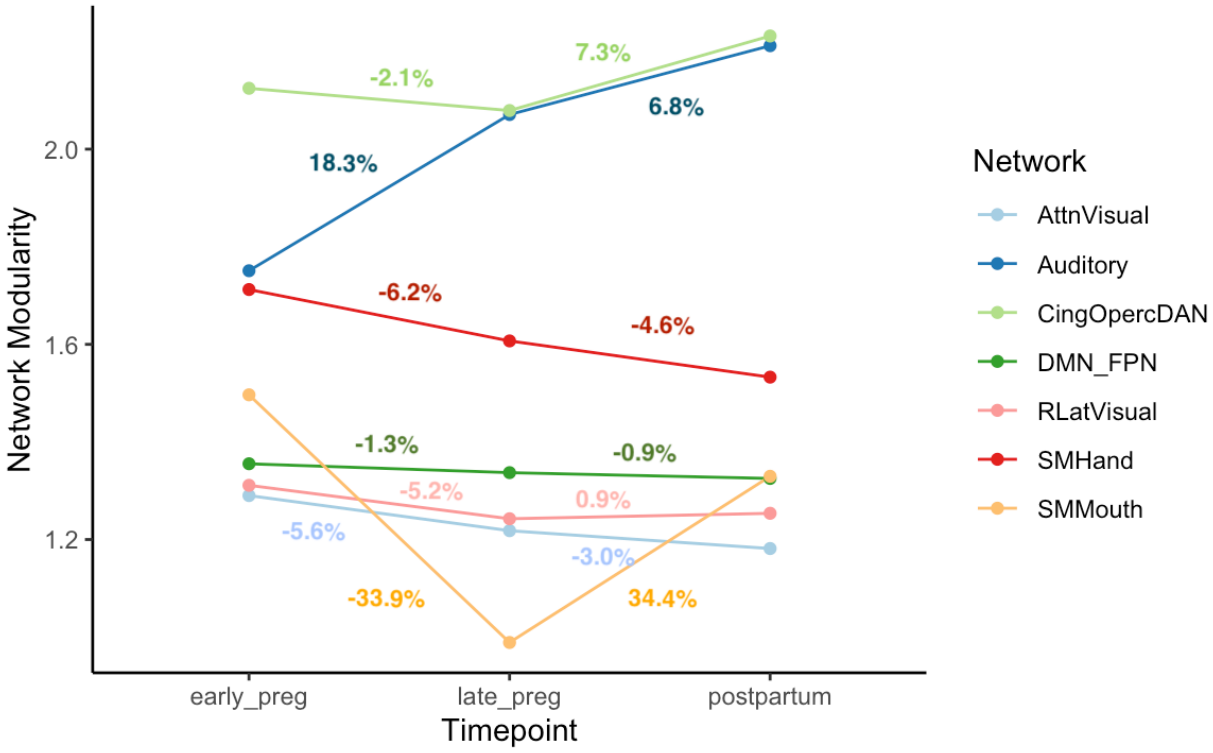

Figure 3. Changes in Mean Network Modularity Across Binned Timepoints

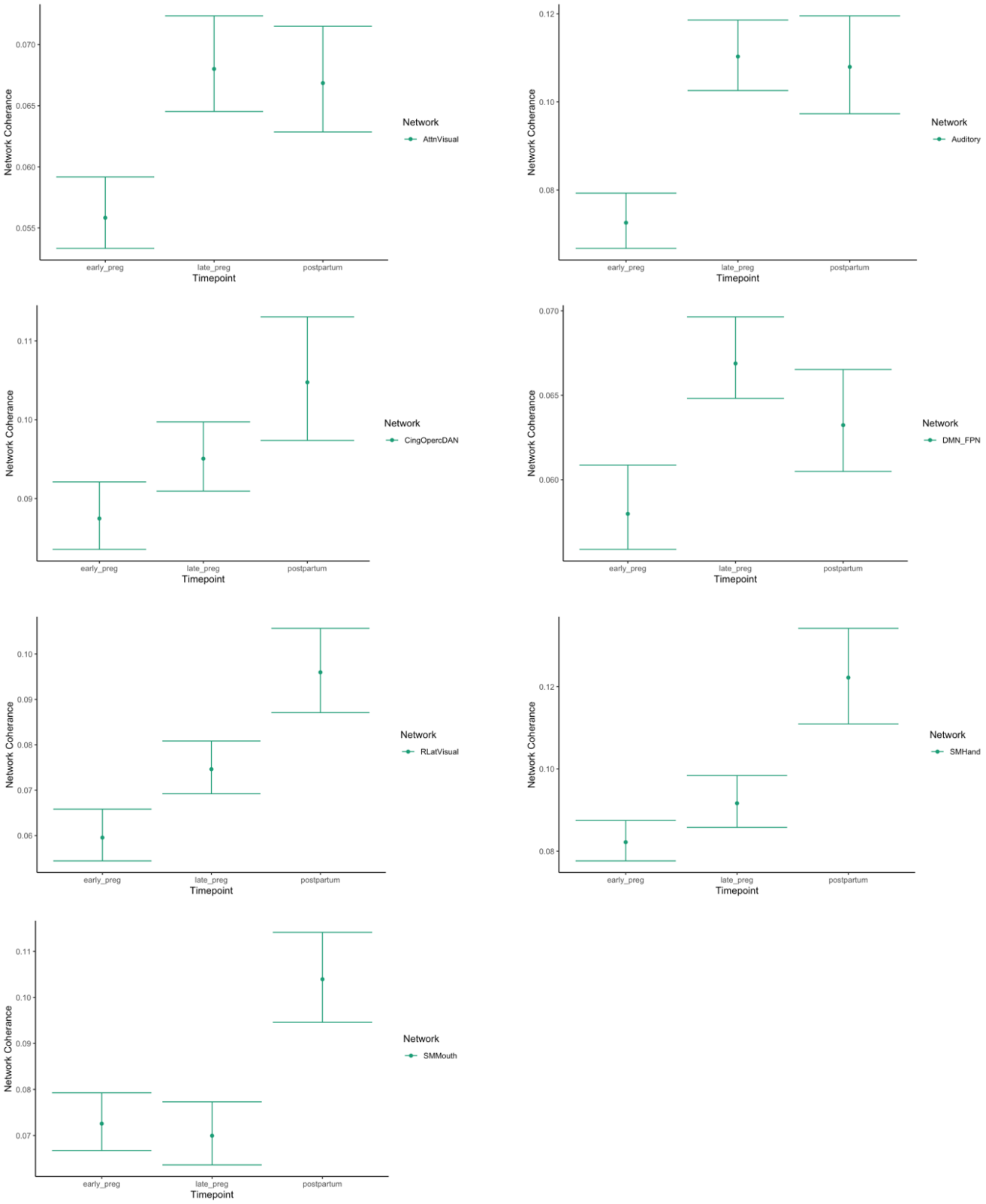

Figure 4. 95% Confidence Intervals for Mean Network Coherence for Binned Timepoints

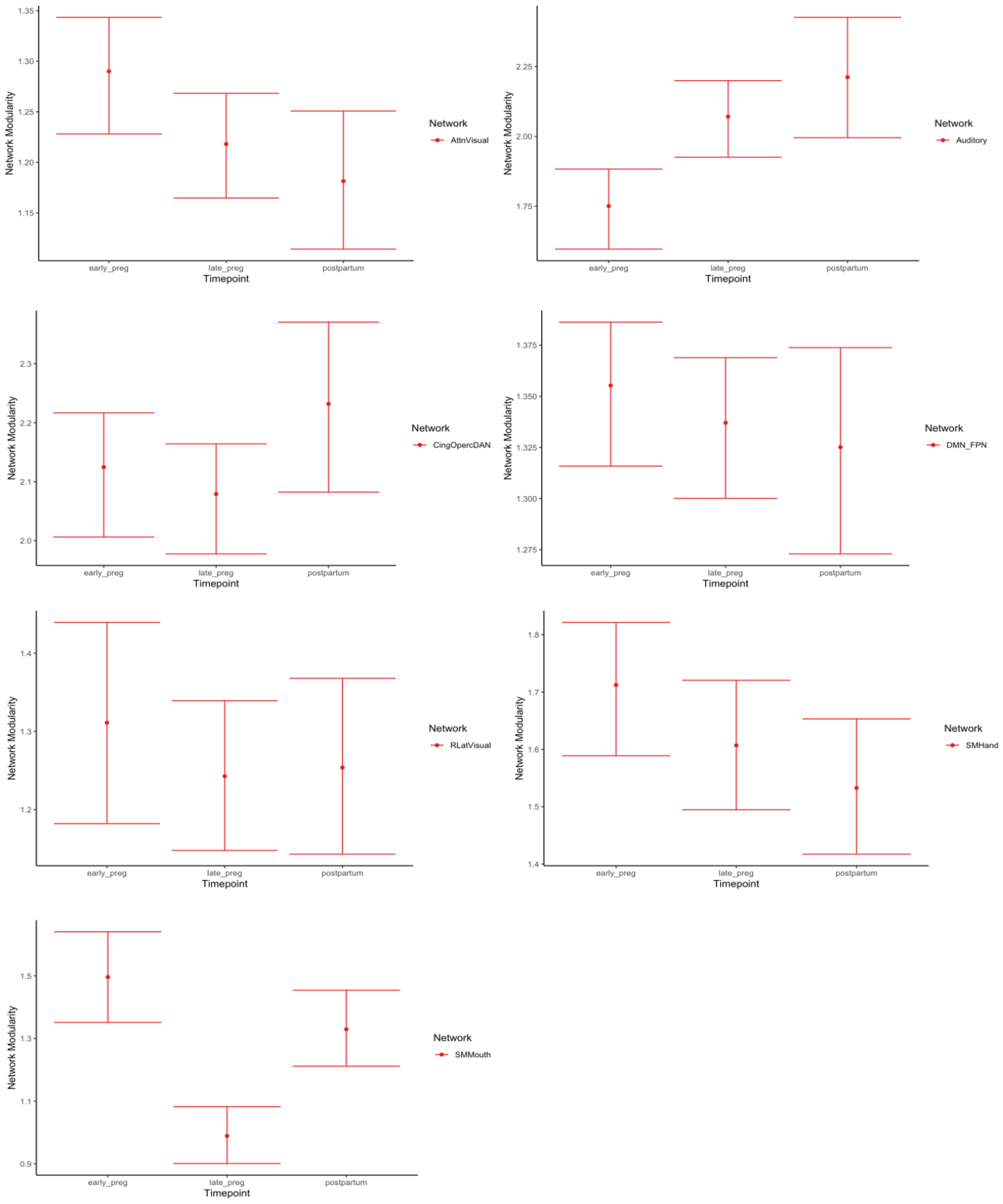

Figure 5. 95% Confidence Intervals for Mean Network Modularity for Binned Timepoints

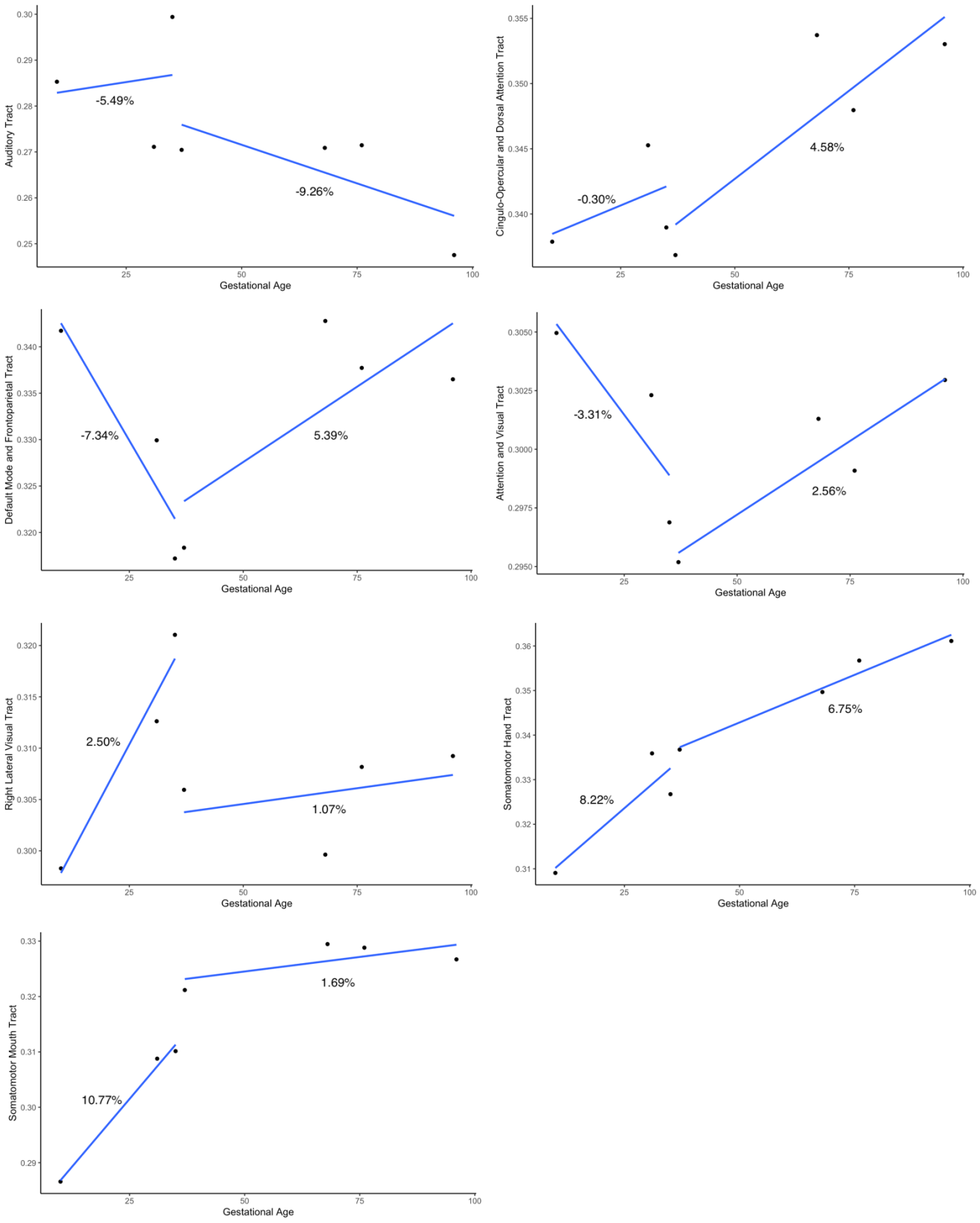

Figure 6. Changes in Fractional Anisotropy as a Function of Gestational Age

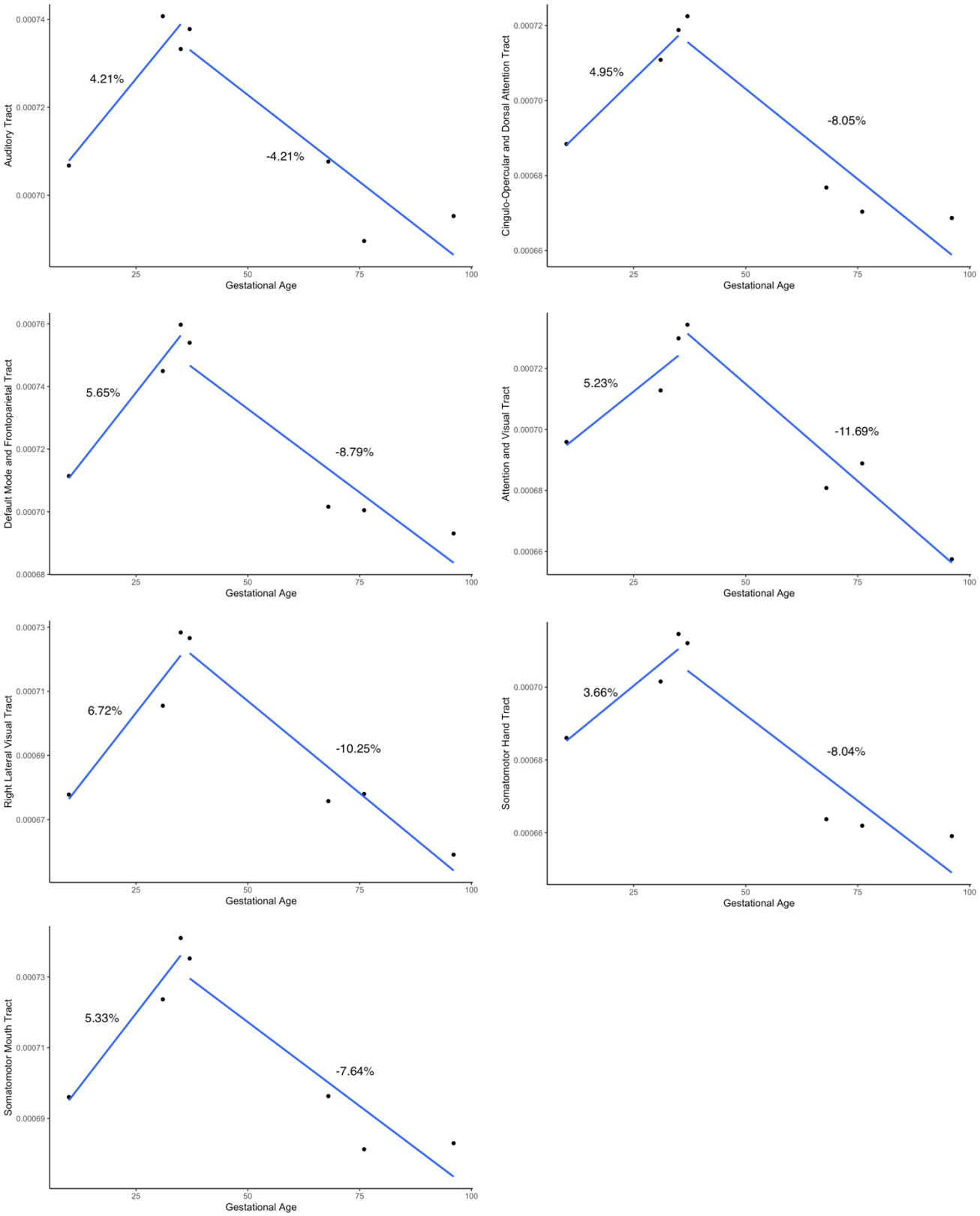

Figure 7. Changes in Mean Diffusivity as a Function of Gestational Age